Calculation of unbalanced magnetic pull in induction machines through empirical method

Calculation of Unbalanced Magnetic Pull in Induction Machines through Empirical Method

H. Chuan*, J. K. H. Shek

Institute for Energy Systems, School of Engineering, The University of Edinburgh, United Kingdom
*H.Chuan@ed.ac.uk

Abstract: Unbalanced Magnetic Pull (UMP) is an important factor to study to improve the reliability of induction machines. UMP occurred in a machine when the existence of rotor eccentricity which causes an uneven distribution of magnetic flux in the airgap. In this study, a UMP damping coefficient is introduced to explain the UMP damping effect from the counteracting flux produced by a parallel connected cage rotor. An empirical method is proposed to calculate the UMP using the damping coefficient and an analytical model. Using the proposed method, a 4-pole and 8-pole squirrel cage induction machine with static eccentricity are investigated, which uses inputs from both Finite Element Analysis and experimental work. Then, the UMP calculation for a dynamic eccentricity with the extracted parameters is done to verify the empirical method. A slip control method is described which uses a UMP/Torque ratio to find the operating slip with the lowest UMP. Comparisons between results with and without slip control are made on both induction machines. It shows that great reduction of UMP can be achieved when the machine is lightly loaded.

1. Introduction

The reliability of electrical machines has become increasingly important, especially with the growth in offshore renewable energy. Failures in offshore wind, wave and tidal current devices are susceptible to longer downtime as they are usually more inaccessible for carrying out maintenance. The downtime for electrical generators is particularly significant, which can lead to a large reduction in revenue [1]. For induction machine, bearing-related failures account for around 40% of the total failures of induction machines [2]. Bearing failure is mainly caused by an increase in bearing wear, in which UMP is one of the contributing factors. UMP causes an additional radial load to be exerted on the bearing, which will reduce the bearing lifetime. In addition, UMP also reduces the overall system stiffness which would amplify vibrations within the system [3].

The two main types of electrical generator used in offshore wind energy are the squirrel cage induction machine (SCIM) and the wound rotor induction machine (WRIM). As reported in [4], they can be found in more than 90% of the turbines in offshore wind farms. As induction machines possess a relatively small airgap, they are more susceptible to UMP [5]. Since the degree of eccentricity is a function of the magnitude of UMP, a slight misalignment in the rotor shaft will cause the production of radial forces. Subsequently, UMP from the rotor shaft will accelerate bearing wear and cause misalignment to increase. The increased misalignment further increases UMP. This cycle continues to accelerate bearing wear until eventual failure. When a bearing fails, further damage to the machine can occur when the rotor comes into contact with the stator. Therefore, a reduction in UMP is essential to increase the reliability of the induction machines.

There are two types of the rotor eccentricity: static eccentricity and dynamic eccentricity. Both types of eccentricity can exist concurrently. For static eccentricity, the rotor rotates on its own axis but not at the centre of the bore. Static eccentricity is caused by the stator core ovality or incorrect positioning of the rotor and the stator at the assembling stage [6]. A small degree of static eccentricity could exist even in newly manufactured machines due to manufacturing and assembly tolerance [7]. For dynamic eccentricity, the rotor rotates at the centre of the stator bore axis but not on its own axis. Dynamic eccentricity is caused by a bent shaft, mechanical resonances at critical speed and bearing wear [8].

In [9], the author shows that the UMP in SCIMs is 80% lower than WRIMs because of the difference in rotor winding configuration. It has also been shown by Dorrell that the parallel path in the cage rotor produces a counteracting flux to even out the airgap flux which reduces UMP [10]. As the existence of a parallel circuit could reduce the UMP, the use of parallel connected stator windings for UMP damping had been discussed in [11][12]. Other than this, Dorrell proposed the installation of damper windings with pole pair ± 1 of the main windings to reduce UMP in induction machines with series-connected stator windings [13]. With the installation of damper windings, it has been shown that UMP can be reduced drastically in WRIM. However, the effect of damper windings is not significant in SCIM since the cage rotor is already parallel connected. Therefore, the authors proposed a method to further reduce the UMP through rotor slip control by using the non-linear characteristic of UMP over rotor slip [14].

UMP calculation can be categorised into numerical and analytical methods [15]. Numerical methods have better accuracy then analytical methods in calculating the UMP of SCIMs because analytical methods cannot calculate the effect from circulating currents. However, numerical methods are very time consuming and, at present, cannot be used for real-time calculations.

In this paper, a new analytical UMP calculation for SCIMs is presented, which uses an empirical method. A UMP damping coefficient is also proposed, which reflects the UMP damping effect from the circulating currents. The parameters taken from the empirical method is used to find the operating slip with the minimum UMP. Lastly, the SCIM is controlled to operate at the slip with the lowest UMP by changing the rotor flux.

2. Unbalanced Magnetic Pull (UMP)

A radial force in the form of UMP is caused by an uneven distribution of flux in the airgap, which in turn is caused by the uneven magnetic reluctance around the airgap due to an eccentric rotor. As the stator and rotor core are both built of material with high permeability, the overall magnetic reluctance can be represented by the airgap magnetic reluctance. An eccentric rotor contributes to the uneven airgap length around the rotor which leads to uneven magnetic flux distribution.

For a constant axial eccentricity, rotor eccentricity can be divided into static eccentricity and dynamic eccentricity. The generation of UMP had been discussed by many researchers [13][14]. The magnetic flux around the airgap caused by the rotor eccentricity can be shown in (1).

$$\begin{aligned} B &= \sum_{p=1}^{\infty} B^p cos(\omega t + p\theta) \times (1 + \varepsilon_s \cos(\theta) + \varepsilon_d \cos(\omega_r t + \theta)) \\ &= \sum_{P=1}^{\infty} \Big[B^p \cos(\omega t + p\theta) + \frac{1}{2} B^p \varepsilon_s \cos(\omega t + (p-1)\theta) \\ &\quad + \frac{1}{2} B^p \varepsilon_s \cos(\omega t + (p+1)\theta) \\ &\quad + \frac{1}{2} B^p \varepsilon_d \cos\big((\omega + \omega_r)t + (p+1)\theta\big) \\ &\quad + \frac{1}{2} B^p \varepsilon_d \cos\big((\omega - \omega_r)t + (p-1)\theta\big) \Big] \end{aligned} \tag{1}$$

Where, B is the amplitude of the magnetic flux density, p is the pole pair number, ω is the supply frequency, ε_s is the degree of static eccentricity, ε_d is the degree of dynamic eccentricity and ω_r is the rotor rotational speed. Meanwhile, ε_d is a function of time and ε_s is a constant value. Both ε_s and ε_d is directionless. (1) has shown that an additional pole pair ± 1 is produced when eccentricity existed in the machine. The pole pair ± 1 flux produced is sideband of every pole-pair flux of a concentric rotor which mainly include fundamental magnetising flux and airgap leakage flux. Harmonics of the airgap leakage flux primary consists of belt harmonics, rotor and stator slots harmonics.

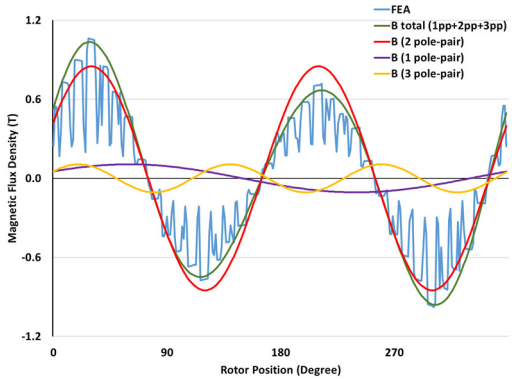

Fig. 1 *Magnetic flux density around the airgap of a 4-pole SCIM at 30% static eccentricity towards the +y direction*

Fig. 1 shows the airgap flux from FEA and the summation of the fundamental magnetic flux harmonics and its pole pair ± 1 flux at an instantaneous time. FEA is done with static simulation where the induced rotor current is not under consideration. As fundamental magnetic flux harmonics is the main flux in the airgap, the summation of fundamental magnetic flux and its pole pair ± 1 flux is approaching the FEA results. However, higher harmonic magnetic flux or the airgap leakage flux should also be included in the analytical model to get an accurate flux distribution calculation when the induction machine is loaded.

After understanding the airgap flux distribution, Maxwell Stress Tensor is used to calculate the force exerted on each point of the rotor with the magnetic flux density distribution information from (1). UMP can be calculated by the integration of the Maxwell Stress Tensor around the rotor circumference which is shown in (2).

$$UMP = \frac{rL}{2\mu_0} \int_0^{2\pi} \left(B'(\theta, t) \right)^2 \cos(\theta)\, d\theta \tag{2}$$

Where, r is the radius of the airgap. L is the axial length of the machine. The $\cos(\theta)$ in (2) is providing the direction information of the flux. Airgap magnetic flux can be separated as forward and backward rotating magnetic flux. In (1), ω for forward rotation has a positive value and ω for backward rotation flux has a negative value.

Two assumptions had been made for the calculation for low degree of eccentricity. Firstly, only first order permeance harmonics is considered. Secondly, the degree of eccentricity is linearly proportional to the pole pair ± 1 flux. Substituting (1) into (2) can be written as (3).

$$\begin{aligned} UMP &= \frac{\pi r L \varepsilon_s}{2\mu_0} \sum_{p=1}^{\infty} B^{p\,2} (1 + \cos(2\omega t)) \\ &\quad + \frac{\pi r L \varepsilon_d}{4\mu_0} \sum_{P=1}^{\infty} B^{p\,2} (\cos(\omega_r t) + \cos((2\omega - \omega_r)t)) \\ &\quad + \frac{\pi r L \varepsilon_d}{4\mu_0} \sum_{P=1}^{\infty} B^{p\,2} (\cos(\omega_r t) + \cos((2\omega + \omega_r)t)) \end{aligned} \tag{3}$$

From (3), the interaction between each pole pair magnetic flux harmonic with its pole pair ± 1 flux sideband produces UMP. The first term of UMP is caused by static eccentricity, the static eccentricity UMP has a constant component and 2 times supply frequency component. The constant component of the UMP is caused by the interaction between two fluxes with the same rotational direction. For the 2 times supply frequency component, which is produced by the interaction between two fluxes with the opposite rotational direction. If the entire magnetic circuit in the induction machine is series connected, the fundamental backwards rotational flux will be damped. For the 2nd and 3rd term, they are UMP caused by dynamic eccentricity, so, the rotor rotational speed is included in the formula. Like the static eccentricity UMP, the first part of 2nd and 3rd terms are caused by the interaction of same rotational direction flux and the second part is caused by the opposite rotational direction flux.

From (3), the UMP is a function of the machine dimension, the degree of eccentricity and the magnetic flux

amplitude for each pole-pair number. Due to the reason that only the magnetic flux that crosses the airgap will contribute to the UMP, it is difficult to estimate the distribution of the airgap flux. Therefore, the magnetic flux that crosses the airgap can be divided into 2 categories: fundamental magnetising flux and airgap leakage flux (higher space harmonics magnetic flux). The challenges here is to calculate the magnitude of the airgap leakage because it is affected by many aspects like airgap length, slot width, winding configuration and rotor angle. So, an empirical method is proposed in Section 5 to find the airgap leakage flux.

3. UMP Damping Effect

The damping of UMP is only applicable for SCIM because the parallel-connected cage rotor could produce a counteracting flux to even out the magnetic flux in the airgap. The UMP damping occurred in the cage rotor when the additional pole pair ±1 magnetic flux is not rotating at the same speed as the rotor. The UMP damping effect only eligible for the magnetising flux. As airgap leakage flux does not cut through the rotor bar, the counteracting flux could not be produced to damp the UMP. Therefore, the UMP caused by the higher space harmonic flux increased when the load current increased.

The UMP damping effect of the cage rotor can be described as an RL circuit. The additional pole pair ± 1 stator rotating flux, ${\lambda_s}^{p\pm1}$, cuts through the rotor bar and induces voltage across the rotor bar. The current that flows in the rotor bar will produce its own rotating flux, ${\lambda_r}^{p\pm1}$, that caused a counteracting force produced to damp the force produced by ${\lambda_s}^{p\pm1}$. This damping is determined by the resultant vector between the ${\lambda_r}^{p\pm1}$ and the ${\lambda_s}^{p\pm1}$ (see Fig. 2). The angular difference can be determined by the rotor current phase shift.

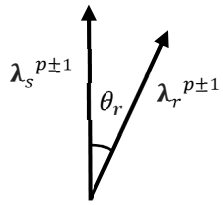

Fig. 2 *Phasor Diagram of the* $\boldsymbol{\lambda_s}^{\boldsymbol{p\pm1}}$ *and* $\boldsymbol{\lambda_r}^{\boldsymbol{p\pm1}}$

The full equation of the resultant magnetic flux after damping is shown in (4).

$$\lambda'_{p\pm1} = {\lambda_s}^{p\pm1}\sqrt{1+\left(\frac{\omega_{slip}k_\sigma L_r}{\sqrt{{R_r}^2+(\omega_{slip}L_r)^2}}\right)^2 - 2\frac{\omega_{slip}k_\sigma L_r}{\sqrt{{R_r}^2+(\omega_{slip}L_r)^2}}\cos\theta_r} \quad (4)$$

Where, ω_{slip} is the angular frequency difference between the angular frequency of ${\lambda_s}^{p\pm1}$ and the rotor angular frequency, i_r is the rotor current, R_r is the rotor resistance, L_r is the rotor inductance, $\lambda'_{p\pm1}$ is the magnetic flux resultant magnitude, θ_r is the angular difference between ${\lambda_s}^{p\pm1}$ and ${\lambda_r}^{p\pm1}$ and k_σ is the flux coupling factor which is shown in (5).

$$k_\sigma = \frac{L_r - L_\sigma}{L_r} \quad (5)$$

Where L_σ is the leakage inductance. The leakage inductance varies with the slip frequency [16]. The imperfect flux coupling means that $\lambda_{p\pm1}$ will not be completely damped. In (6), the damping coefficient, β, is introduced to show the UMP damping effect of the SCIM.

$$\beta = \sqrt{1+\left(\frac{\omega_{slip}k_\sigma L_r}{\sqrt{{R_r}^2+(\omega_{slip}L_r)^2}}\right)^2 - 2\frac{\omega_{slip}k_\sigma L_r}{\sqrt{{R_r}^2+(\omega_{slip}L_r)^2}}\cos\theta_r} \quad (6)$$

From (6), the amount of flux damped is based on the ω_{slip} of the pole pair ±1 flux. Furthermore, θ_r is also a function of the slip frequency because the reactance of the circuit is increased when the frequency is increased. The damping coefficient is affected by the changing of slip frequency. Therefore, the pole pair number and the rotor slip will affect the damping coefficient (see Fig. 3).

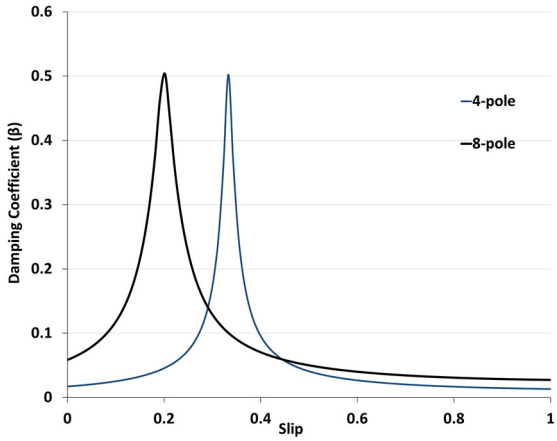

Fig. 3 *Damping coefficient for 4-pole and 8-pole SCIM at different rotor slip*

4. Experimental and FEA results

4.1. Experimental Setup

An 8-pole, 5.5kW, 400V, SCIM was used in the experimental testing. The SCIM is connected to a permanent magnet machine through a torque transducer. The permanent magnet machine is then connected to a resistive load bank. The machine setup is shown in Fig.3.

For the experiments, the rotor is set to 20% static eccentricity. The stator and the rotor are separated by removing the end caps of the SCIM. The rotor is supported by external bearings which are mounted directly to the base frame. The stator is mounted to the force plate, which in turn is bolted to the base frame. The UMP is measured from the force exerted on the force plate by the stator. Kistler 9366CC multi-component force sensors were used for the force plate.

The machine was tested at a reduced voltage to minimise the effect of saturation. The full load rating of the machine decreases when the voltage decreases. The machine has a full load rating at a slip value of 0.05. The voltage was set to 0.5pu and 0.35pu for both the experiments and the simulations. The UMP for each load was recorded for 15 seconds. Then, the experimental results were analysed using FFT analysis for each slip value. For static eccentricity, from (3), there is a constant UMP and a 2x supply frequency force. The 100Hz frequency force is relatively small (<10%) if compared to the constant component. Therefore, only the constant component from the FFT analysis is extracted for the

analysis in this paper. The UMP is recorded when the machine reached steady state, so, only the UMP in the induction machine stable operating region is analysed.

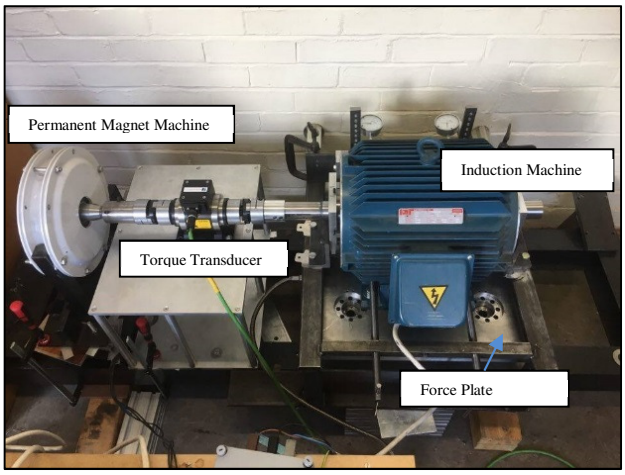

Fig. 4 *Experimental Setup*

Table 1 Parameters of the SCIM

	8-pole SCIM	4-pole SCIM
Power, kW	5.5	7.5
Poles	8	4
Axial length, mm	180.0	178.6
Stator diameter, mm	120	140
Rotor diameter, mm	78.00	89.75
Airgap length, mm	0.9	0.5
Stator slots	52	36
Stator turns per coil	13	22
Stator resistance (phase), Ω	1.579	1.08
Rotor slots	42	28
Rotor turns per coil	1	1
Rotor resistance (phase), Ω	0.846	1.105
Stator inductance (phase), H	0.1795	0.282
Leakage factor	0.18	0.11
Rotor inertia, kg/m^3	0.0804	0.1296

4.2. FEA

Instead of using the analytical model to calculate the UMP, FEA is used due to its higher accuracy when higher space harmonics exist. In addition, the existence of the parallel path of the cage rotor makes the analytical calculation of UMP more complicated because the cage rotor bars are not pole specific. FEA calculates electromagnetic problems through subdivision of the whole induction machine into smaller parts called finite elements. The process is very time consuming and requires significant computational power. Therefore, the geometry of the induction machine can be simplified as a 2D model which assumes that the axial direction of the induction machine has the constant geometry. Infolytica MagNet was used for analysis of a 4-pole and an 8-pole SCIM. The FEA model of the 8-pole SCIM is based on the experimental machine. The specification of both machines is shown in Table 1.

4.3. Results

In Fig. 5, 20% of static eccentricity is set on both SCIM. Good correlation has been shown between the experimental and the FEA results (See Fig. 5(b)). The results for both SCIMs had shown that the UMP is a quadratic function with a constant offset when the SCIM running in its operating region (See Fig. 5). As the magnetizing flux is almost constant in the SCIM operating region, the constant offset component of the UMP is caused by the magnetising flux. Then, the quadratic increment of UMP is caused by the airgap leakage flux because UMP is a square function of current. The stator and rotor current has a linear relationship with the slip, so, the airgap leakage flux of the SCIM increased when the slip increased.

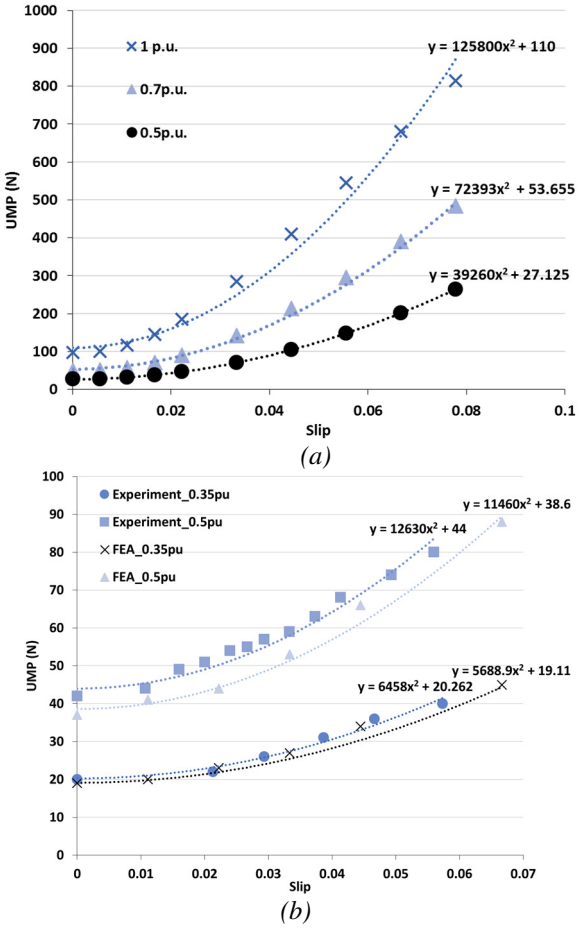

Fig. 5 *UMP at different rotor slip for (a) 4-pole (b) 8-pole SCIM with 20% static eccentricity*

5. Empirical Method

As the overall UMP is a function of slip or current, an empirical method is proposed to find the parameters to use for UMP calculation. To extract the unknown parameters, a set of UMP data with the same rotor eccentricity at different load is needed. The set of data can be either FEA or experimental results. In addition, the damping coefficient of the SCIM at different load need to be calculated from (6). From the collected data, the parameters for the UMP that caused by magnetising flux and airgap leakage flux can be found. Then, these parameters found from the proposed empirical method can be used to find the UMP for different

rotor eccentricity, excitation voltage and load. As the core saturation is neglected in the empirical method, it is only applicable for rotor with low degree of eccentricity and operates within its rated slip.

In Section 5.1, the experimental and FEA results from Fig. 5 are used to find the unknown parameters for UMP calculations by using the proposed empirical methods. With the parameters extracted from Section 5.1, UMP of the 4-pole SCIM with 10% dynamic eccentricity at different load is calculated in Section 5.2. Then, FEA results are used to verify the proposed empirical method.

5.1. Static eccentricity

The FEA and experimental results from Fig. 5 is used to find the parameter of the UMP caused by the airgap leakage flux. When the stator resistance and leakage reactance are considered, the fundamental magnetising flux decreases as the slip increases. Meanwhile, the UMP damping coefficient increases as the slip increases (see Fig. 6(a)). The rate of change for both UMP damping coefficient and fundamental magnetising flux is highly dependent of the machine's parameters. For the 4-pole SCIM, multiplication of its UMP damping coefficient with the square of the fundamental magnetizing flux can be assumed to be constant when the machine running in its operating region (see Fig. 6(b)). When multiplication is assumed to be constant, both the UMP damping coefficient and the fundamental magnetic flux density can be assumed to be constant. For a constant fundamental magnetic flux density, the stator resistance, stator leakage reactance and rotor leakage reactance can be neglected. This assumption can also be applied to the 8-pole SCIM in this paper.

The UMP model shown in (3) is a current fed model to calculate the magnetic flux where the calculation can be done after getting the current information. In the simplified model, $I_S = I_M + I_R$. The whole simplified UMP equation can be written as (7) at any instant in time. The airgap leakage inductance for the stator and the rotor are assumed to be the same. Also, the airgap leakage inductance can be assumed to be constant in the machine's operating region [16].

$$UMP = K\left[(\beta L_M I_M)^2 + (L_{ag} I_M)^2 + (L_{ag} I_R)^2 + (L_{ag} I_R)^2\right] \quad (7)$$

Where the constant $K = \frac{\varepsilon_s + \varepsilon_d(\cos \omega t)}{8\mu_0 \pi r L}$, L_M is the magnetising inductance and L_{ag} is the airgap leakage inductance. Changing the current fed model in (7) into voltage fed in (8).

$$UMP = 2Ks^2v^2\left(L_{ag}\frac{E}{R_r}\right)^2 + Kv^2\left[\beta(L_M I_M)^2 + \left(L_{ag} I_M\right)^2\right] \quad (8)$$

$$\text{Let, } A = 2Ks^2\left(L_{l_{ag}}\frac{E}{R_r}\right)^2$$

$$B = K\left[\beta\left(L_M\frac{E}{X_M}\right)^2 + \left(L_{ag}\frac{E}{X_M}\right)^2\right]$$

Where, s is the rotor slip, E is the rated excitation voltage. *v(pu)* term is added in (8) to standardize the equation for different excitation voltage. Therefore, A is the parameter for the UMP caused by airgap leakage flux from load current. Meanwhile, B is the parameter for the UMP primarily caused by magnetising flux; airgap leakage flux from the magnetising current can be neglected. Table 2 shows the curve fitting results simulated from Figure 5(b). The curve fitting includes only the constant component and a square component to match the A and B. Curve fitting does not provide the most accurate results where there is a range of constants that could fit in the A and B values. However, this error will not significantly affect on the overall pattern of the UMP. The average of the values can be taken to predict the UMP of the SCIM.

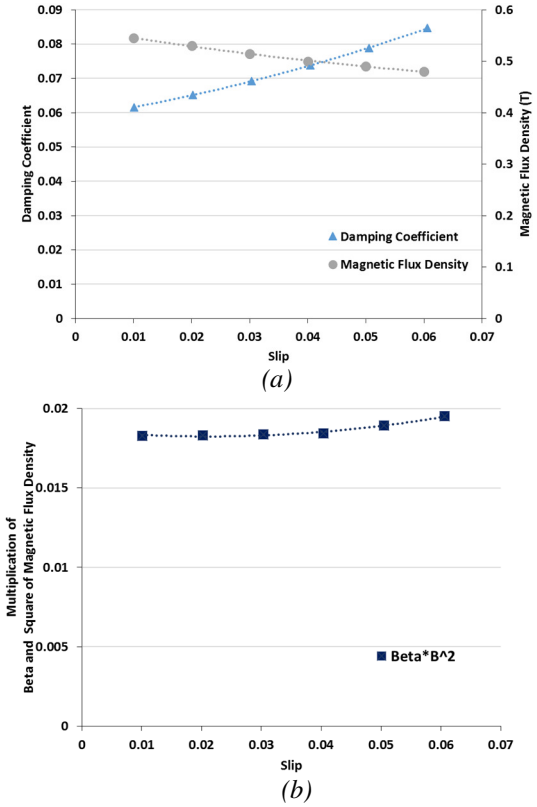

Fig. 6 *(a) Damping coefficient and the fundamental magnetising flux density of the 4-pole SCIM (b) Multiplication of damping coefficient and square of the fundamental magnetising flux density*

From Table 2, for the 4-pole SCIM, when the voltage increases, the A value decreases, meanwhile, the B value remains almost the same. The decrement of value A is due to magnetic saturation. The 0.5pu and 0.7pu cases have a much closer value A than the 1.0pu case. This is because the airgap leakage inductance is greatly affected by the magnetic saturation.

For the 8-pole SCIM, the FEA results are slightly lower than the experimental results for both 0.35pu and 0.5pu (See Fig. 5(b)). As the FEA is simulated in a 2-Dimension model, the skew rotor is not under consideration. Therefore, the B value of the FEA results has a lower value than the experiment. The smaller B value is caused by the reduced damping effect from the SCIM because the main UMP in B is from the fundamental magnetizing flux. Then, the slightly lower A value of the FEA than the experimental result is caused by increment in airgap leakage flux which is contributed by the skew leakage flux. Furthermore, the FEA and experimental results at different supplied voltage are almost the same. This is because the low supplied voltage does not cause magnetic saturation in the iron core.

Comparing the FEA results of the 4-pole and 8-pole SCIM, even though both machines have almost the same

machine volume, peak magnetic flux and eccentricity, the *B* value of the 8-pole machine is 50% higher than the 4-pole machine. Higher rotor slip angular frequency would increase the damping of UMP (see Fig. 3). However, the *A* value of the 4-pole machine is 3 times higher than the *A* value of the 8-pole machine. The difference is mainly come from the airgap difference between both machines where the 8-pole machine has a 0.8mm airgap and the 4-pole machine has a 0.5mm airgap.

Table 2 *A* and *B* coefficient for 0.5pu and 0.35pu

Machine	Voltage (p.u.)	*A*	*B*	R-squared value
4 pole	0.5	157040	108.48	0.9984
	0.7	147740	109.5	0.9964
	1.0	125800	110	0.9840
8 pole	0.35 (FEA)	46440	156	0.9910
	0.5 (FEA)	45840	154.4	0.9753
	0.35 (Exp)	52718	165.4	0.9787
	0.5 (Exp)	50520	176	0.9665

5.2. Dynamic Eccentricity

This section is to verify the extracted parameters in Table 2. UMP estimation of the 4-pole SCIM with 10% dynamic eccentricity is done. As the damping coefficient of dynamic eccentricity is different from static eccentricity, the assumption of constant damping coefficient and constant magnetic flux density in Section 4.4 cannot be used. As the degree of eccentricity is assumed to have a linear relationship with the UMP, the parameters taken from Table 2 (20% eccentricity) is divided by 2. Furthermore, a reduction factor of magnetising flux is combined with the damping coefficient (see Fig. 7(a)). Then, the airgap leakage flux caused by the magnetising current is neglected. The new parameters are shown in Table 3.

FEA is used to verify the calculated UMP (see Fig. 7(b)). Although there is a slight difference between the estimated UMP and the UMP from FEA, the overall pattern of the UMP is almost the same. The main difference might come from the different UMP damping effect of the stator belt harmonics magnetising flux. Furthermore, the airgap leakage flux may have slight changes due to the dynamic eccentricity.

Table 3 Parameters for the 4-pole SCIM with 10% dynamic eccentricity

Voltage (p.u.)	*A*	*B*	β_{new}
1.0	67500	447	$191.9s^2 - 23.7s + 1$

5.3. Discussion

The key to implement the empirical method is the calculation of the UMP damping coefficient. For WRIM with series connected stator windings, the damping coefficient part can be set into 1 because there is no counteracting flux produced to damp the UMP. If the WRIM has parallel connected stator windings, the damping coefficient need to be recalculated based on numbers of parallel stator windings. The damping coefficient calculation from (6) is based on the assumption of infinite parallel windings that is more applicable for a cage rotor because there is each cage rotor bar is parallel connected. As shown in Table 2 that the core saturation will slightly affect the UMP, the accuracy of the empirical method can be improved if a saturation model is added in the calculation.

The main advantage of using the proposed empirical method is its robustness. The proposed empirical method can be used on any types of WRIM or SCIM as long as there is a set of UMP data. Other than this, the empirical method has a fast computational time. Real-time UMP estimation could be implemented if the rotor eccentricity is known. When implementing flux optimisation to improve the efficiency of induction machines, the empirical methods can be used to calculate the additional bearing friction loss caused by UMP. Furthermore, it can also be used to estimate the bearing lifetime.

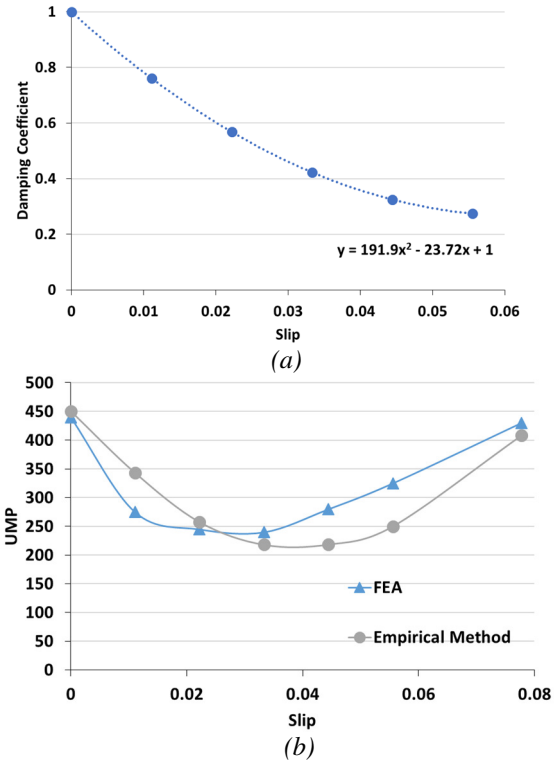

Fig. 7 *(a) New damping coefficient (b) UMP of a 4-pole SCIM with 10% dynamic eccentricity*

6. Slip Control Method to reduce UMP

Slip control methods are often used to increase the efficiency of a lightly loaded induction machine [17]. Induction machines are most efficient when running at its rated slip. By reducing the magnetizing flux, the rated load can be reduced. However, changing the magnetizing flux is not suitable for situations that need fast response since changing the rotor flux may take a few hundred milliseconds. The response time depends on the amplitude of changes and the rotor time constant of the machine.

Due to the nonlinear characteristic of UMP versus slip, as shown in Fig. 5, there is clearly a specific operating rotor slip that results in minimum UMP. Therefore, the

UMP/torque ratio (γ) is introduced to find the slip with the lowest UMP for a machine to operate.

As the saturation effect on the airgap leakage flux is not significant at low slip (rated slip is 0.05), the three different excitation voltages have around the same minimum UMP/Torque ratio (see Fig. 8(a)). As the slip further increases, the difference of the UMP/Torque ratio for each case started to increase because of the slight core saturation. Meanwhile, the ratio is the same for both cases in Fig. 8(b) because only 0.35pu and 0.5pu are investigated. However, the amount of saturation is still highly dependent on the machine design.

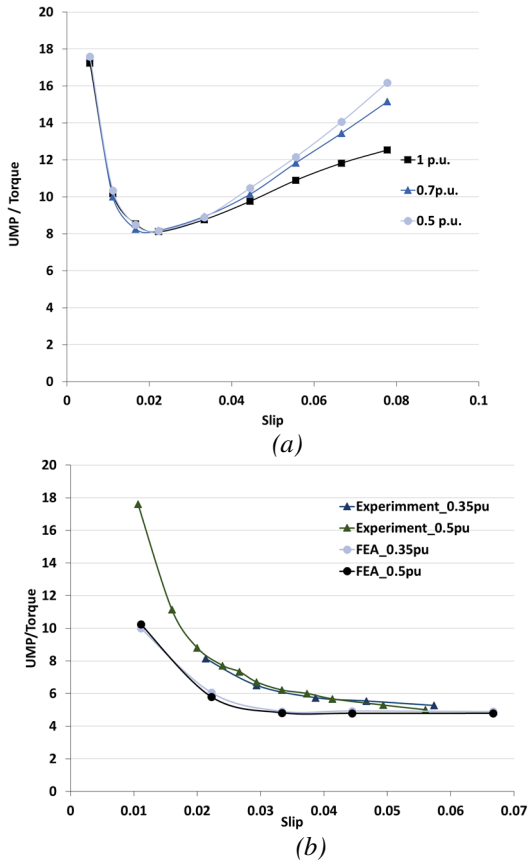

Fig. 8 *UMP/Torque ratio for (a) 4-pole (b) 8-pole SCIM*

Assuming that the slip is linearly proportional to the torque, the relationship between torque and slip can be written as (9). The derivation from (9) to (10) is to calculate the slip with the minimum UMP.

$$\gamma = \frac{A}{k_t} s + \frac{B}{k_t s} \tag{9}$$

Where, k_t is the constant of the machine. Differentiation of (9) with $\frac{d\gamma}{ds} = 0$ is set to get the minimum UMP/Torque. The slip with the lowest UMP for the same torque can be given as (10).

$$s = \sqrt{\frac{B}{A}} \tag{10}$$

Table 4 shows the slip with lowest UMP by using (10) with the ***A*** and ***B*** value taken from the FEA results at 0.5pu rated voltage. The optimum value is different for different machines design which will affect the ***A*** and ***B*** value.

Table 4 Summary of the slip with lowest UMP

Machine 1	B/A	Slip
4-pole	0.0006877	0.026
8-pole	0.00356	0.058

The rotor slip can be controlled by changing the rotor flux. Either scalar control or vector control can be used in the rotor flux control. If the machine is running at fixed load, changing the rotor flux by using the scalar control or by using the vector control have almost the same converging time when the model-based method is used in finding the optimum flux [18]. For scalar control (Voltage/Hertz control), magnetizing flux can be changed by changing the ratio of V/f.

$$T = \frac{3}{2n_s} \times \frac{sE^2}{R_r} \tag{11}$$

Where, n_s is the synchronous rotating frequency which is a function of number of pole pairs and the supply frequency. (11) shows the simplified torque calculation which neglects the leakage reactance due to low slip frequency. For scalar control, after knowing the torque and the speed information of the machine, (11) can be used to find the magnitude of the desired voltage to achieve 0.05 slip. The desired voltage cannot be higher than the rated voltage because most electrical machines is designed to operate at the knee point of the BH curve; this may lead to core saturation when the excitation voltage is beyond the rated voltage. Therefore, slip control method is only applicable for lightly loaded machines.

For the vector control, instead of adjusting the supplied voltage, after getting the desired voltage from (11), the magnetizing current needs to be calculated as an input variable for the vector control system. The current can be calculated by using (12).

$$E = L_M \frac{dI_M}{dt} \tag{12}$$

In Fig. 9, the comparison is made between with and without slip control by using the proposed empirical method from no load to full load. It shows that the impact of slip control is diminished as the load increases. As the 8-pole machine has an optimum slip that is higher than the rated slip, the UMP can be reduced at every load except its full load. Meanwhile, the UMP of the 4-pole machine can only be reduced when the load is below 20Nm because the 4-pole SCIM has a lower optimum slip.

The slip control method is more effective when the SCIM is lightly loaded. For example, offshore wind turbines operate above 50% capacity factor for only 34% of the time. Also, the average capacity factor of an offshore wind turbine is around 36% [19]. Similarly, tidal current turbines and wave energy converters rarely operate at full load due to the nature of the variable energy source. The capacity factor for both tidal current and wave energy is around 35%-40% [20]. Therefore, the slip control method can be useful for certain application to increase the efficiency and also to reduce the UMP.

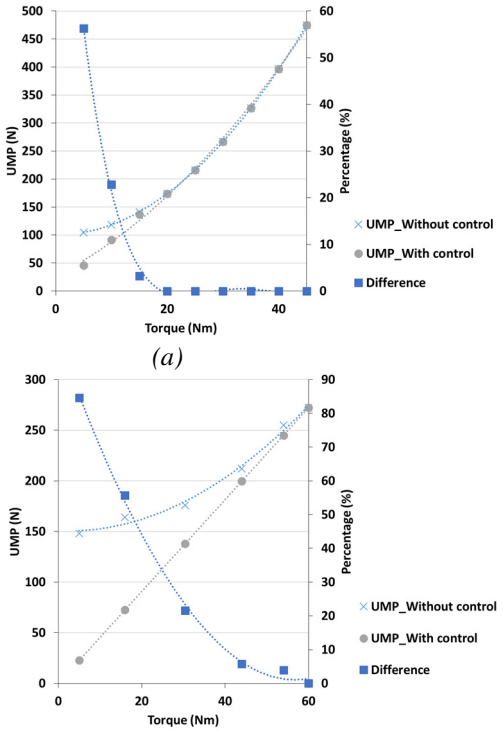

Fig. 9 *Comparison between with and without slip control for (a) 4-pole (b) 8-pole SCIM*

7. Conclusion

Using empirical method to calculate the UMP based on the proposed UMP damping coefficient is presented. The fast computational time of analytical calculation is the main reason of using the empirical method. In the empirical method, the UMP caused by the magnetising flux and airgap leakage flux are separated. The parameters for UMP calculation can be found from either experimental or FEA results. Examples of a 4-pole and 8-pole SCIMs are shown. The extracted parameters from the empirical method are affected by the design of the machines. For example, UMP caused by the airgap leakage flux is higher when the airgap length is shorter. With the extracted parameter from the FEA results of static eccentricity, calculation of the UMP of dynamic eccentricity had been done to verify the proposed empirical methods.

In order to implement a control system to reduce UMP, a UMP/Torque ratio is introduced to find the slip with the lowest UMP. With the extracted parameter from the empirical method, calculation of the optimum operating slip is shown. Finally, the comparison had been made on both SCIMs for the case with and without slip control. Results have shown that the UMP is greatly reduced when the SCIM is lightly loaded.

8. References

[1] M. Shafiee, “Maintenance logistics organization for offshore wind energy: Current progress and future perspectives,” *Renewable Energy*, vol. 77, pp. 182-193, May 2015.

[2] L. M. Popa, B. B. Jensen, E. Ritchie and I. Boldea, "Condition monitoring of wind generators," *38th IAS Annual Meeting on Conference Record of the Industry Applications Conference, 2003.*, 2003, pp. 1839-1846 vol.3.

[3] M. Michon, R. C. Holehouse, K. Atallah, G. Johnstone, "Effect of Rotor Eccentricity in Large Synchronous Machines," *IEEE Transactions on Magnetics*, vol. 50, no. 11, pp. 1-4, Nov. 2014.

[4] Z. Zhang, A. Chen, A. Matveev, R. Nilssen, A. Nysveen, “High-power Generators for Offshore Wind Turbines,” *Energy Procedia*, vol. 35, 2013, pp. 52-61.

[5] A. Burakov, A. Arkkio, "Low-order parametric force model for eccentric-rotor electrical machine with parallel connections in stator winding," *IEE Proceedings - Electric Power Applications*, vol. 153, no. 4, pp. 592-600, Jul. 2006.

[6] J. R. Cameron, W. T. Thomson, A. B. Dow, "Vibration and current monitoring for detecting airgap eccentricity in large induction motors," *IEE Proceedings B - Electric Power Applications*, vol. 133, no. 3, pp. 155-163, May 1986.

[7] D. G. Dorrell, A. Salah, Y. Guo, "The Detection and Suppression of Unbalanced Magnetic Pull in Wound Rotor Induction Motors Using Pole-Specific Search Coils and Auxiliary Windings," *IEEE Transactions on Industry Applications*, vol. 53, no. 3, pp. 2066-2076, May/Jun. 2017.

[8] S. Nandi, H. A. Toliyat, X. Li, "Condition monitoring and fault diagnosis of electrical motors-a review," *IEEE Transactions on Energy Conversion*, vol. 20, no. 4, pp. 719-729, Dec. 2005.

[9] M. Bradford, “Unbalanced Magnetic pull in a 6-pole induction motor,” *Proceedings of Institution of Engineers*, vol.115, Issue 11, Nov. 1968.

[10] D. G. Dorrell, "Sources and Characteristics of Unbalanced Magnetic Pull in Three-Phase Cage Induction Motors With Axial-Varying Rotor Eccentricity," *IEEE Transactions on Industry Applications*, vol. 47, no. 1, pp. 12-24, Jan./Feb. 2011.

[11] D. G. Dorrell, A. C. Smith, "Calculation of UMP in induction motors with series or parallel winding connections," *IEEE Transactions on Energy Conversion*, vol. 9, no. 2, pp. 304-310, Jun. 1994.

[12] A. Burakov, A. Arkkio, "Comparison of the Unbalanced Magnetic Pull Mitigation by the Parallel Paths in the Stator and Rotor Windings," *IEEE Transactions on Magnetics*, vol.43, no.12, pp.4083,4088, Dec. 2007.

[13] D. G. Dorrell, J. K. H. Shek, M. A. Mueller, M. Hsieh, "Damper Windings in Induction Machines for Reduction of Unbalanced Magnetic Pull and Bearing Wear," *IEEE Transactions on Industry Applications*, vol.49, no.5, pp.2206,2216, Sept./Oct. 2013.

[14] H. Chuan, J. K. H. Shek, "Reducing Unbalanced Magnetic Pull of an induction machine through active control," *IET International Conference on Power Electronics, Machines and Drives,* Glasgow, 2016, pp. 1-6.

[15] A. Salah, Y. Guo, D. Dorrell, "Monitoring and damping unbalanced magnetic pull due to eccentricity fault in induction machines: A review," *2017 20th International Conference on Electrical Machines and Systems (ICEMS)*, Sydney, NSW, 2017, pp. 1-6.

[16] Z. Ling, L. Zhou, S. Guo, Y. Zhang, "Equivalent Circuit Parameters Calculation of Induction Motor by Finite Element Analysis," *IEEE Transactions on Magnetics*, vol. 50, no. 2, pp. 833-836, Feb. 2014.

[17] A. G. Abo-Khalil, "Model-based optimal efficiency control of induction generators for wind power systems," *IEEE International Conference on Industrial Technology*, Auburn, AL, 2011, pp. 191-197.

[18] F. Abrahamsen, F. Blaabjerg, J. K. Pedersen, P. Z. Grabowski and P. Thogersen, "On the energy optimized control of standard and high-efficiency induction motors in CT and HVAC applications," *IEEE Transactions on Industry Applications*, vol. 34, no. 4, pp. 822-831, Jul./Aug. 1998.

[19] Department of Business Energy and Industrial Strategy, Digest of United Kingdom energy statistics 2017, [Online]. Available: https://www.gov.uk/government/uploads/system/uploads/attachment_data/file/643414/DUKES_2017.pdf [Accessed: 30/10/2017].

[20] World Energy Resources Marine Energy 2016, [Online]. Available:https://www.worldenergy.org/wpcontent/uploads/2017/03/WEResources_Marine_2016.pdf [Accessed: 28/03/2018].